Dalton Transactions

Cite this: *Dalton Trans.*, 2012, **41**, 13429

www.rsc.org/dalton

PAPER

Strong metal–metal coupling in mixed-valent intermediates [Cl(L)Ru(μ-tppz)Ru(L)Cl]$^+$, L = β-diketonato ligands, tppz = 2,3,5,6-tetrakis(2-pyridyl)pyrazine†

Tanaya Kundu,[a] David Schweinfurth,[b] Biprajit Sarkar,[b] Tapan Kumar Mondal,[c] Jan Fiedler,[d] Shaikh M. Mobin,[a] Vedavati G. Puranik,[e] Wolfgang Kaim*[b] and Goutam Kumar Lahiri*[a]

Received 12th January 2012, Accepted 31st August 2012
DOI: 10.1039/c2dt31763j

Five diruthenium(II) complexes [Cl(L)Ru(μ-tppz)Ru(L)Cl] (**1**–**5**) containing differently substituted β-diketonato derivatives (**1**: L = 2,4-pentanedionato; **2**: L = 3,5-heptanedionato; **3**: L = 2,2,6,6-tetramethyl-3,5-heptanedionato; **4**: L = 3-methyl-2,4-pentanedionato; **5**: L = 3-ethyl-2,4-pentanedionato) as ancillary ligands (L) were synthesized and studied by spectroelectrochemistry (UV-Vis-NIR, electron paramagnetic resonance (EPR)). X-ray structural characterisation revealed *anti* (**1**, **2**, **5**) or *syn* (**3**) configuration as well as non-planarity of the bis-tridentate tppz bridge and strong $d\pi(Ru^{II}) \rightarrow \pi^*$(pyrazine, tppz) back-bonding. The widely separated one-electron oxidation steps, $Ru^{II}Ru^{II}/Ru^{II}Ru^{III}$ and $Ru^{II}Ru^{III}/Ru^{III}Ru^{III}$, result in large comproportionation constants (K_c) of $\geq 10^{10}$ for the mixed-valent intermediates. The *syn*-configurated $\mathbf{3}^n$ exhibits a particularly high K_c of 10^{12} for n = 1+, accompanied by density functional theory (DFT)-calculated minimum Ru–N bond lengths for this $Ru^{II}Ru^{III}$ intermediate. The electrogenerated mixed-valent states $\mathbf{1}^+$–$\mathbf{5}^+$ exhibit anisotropic EPR spectra at 110 K with average values <g> of 2.304–2.234 and g anisotropies $\Delta g = g_1 - g_3$ of 0.82–0.99. Metal-to-metal charge transfer (MMCT) absorptions occur for $\mathbf{1}^+$–$\mathbf{5}^+$ in the NIR region at 1660 nm–1750 nm ($\varepsilon \approx 2700$ dm^3 mol^{-1} cm^{-1}, $\Delta\nu_{1/2} \approx 1800$ cm^{-1}). DFT calculations of $\mathbf{1}^+$ and $\mathbf{3}^+$ yield comparable Mulliken spin densities of about 0.60 for the metal ions, corresponding to valence-delocalised situations $(Ru^{2.5})_2$. Rather large spin densities of about −0.4 were calculated for the tppz bridges in $\mathbf{1}^+$ and $\mathbf{3}^+$. The calculated electronic interaction values (V_{AB}) for $\mathbf{1}^+$–$\mathbf{5}^+$ are about 3000 cm^{-1}, comparable to that for the Creutz–Taube ion at 3185 cm^{-1}. The DFT calculations predict that the $Ru^{III}Ru^{III}$ forms in $\mathbf{1}^{2+}$–$\mathbf{5}^{2+}$ prefer a triplet (S = 1) ground state with ΔE ($S = 0 - S = 1$) ~5000 cm^{-1}. One-electron reduction takes place at the tppz bridge which results in species $[Cl(L)Ru^{II}(\mu\text{-tppz}^{\cdot-})Ru^{II}(L)Cl]^-$ ($\mathbf{1}^{\cdot-}$–$\mathbf{3}^{\cdot-}$, $\mathbf{5}^{\cdot-}$) which exhibit free radical-type EPR signals and NIR transitions typical of the tppz radical anion. The system $\mathbf{4}^n$ is distinguished by lability of the Ru–Cl bonds.

Introduction

Since the discovery of the pyrazine-mediated strong inter-metallic electronic coupling in the mixed-valent ($Ru^{II}Ru^{III}$) state of the Creutz–Taube ion (**A**)[1] there have been continuing initiatives to design new mixed-valent diruthenium(II,III) frameworks using either pyrazine or pyrazine-derived bridges in combination with a variety of ancillary ligands.[2] The primary emphasis has been on theoretical[3] and conceptual[4] advancements as well as on explorations of potential applications in information transfer,[5] energy-relevant research,[6a,b] or for optical devices.[6c]

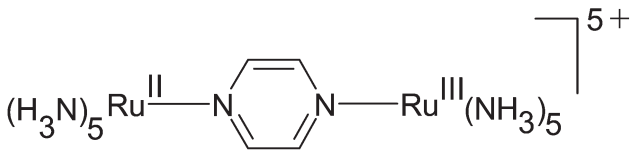

A

[a]*Department of Chemistry, Indian Institute of Technology Bombay, Powai, Mumbai-400076, India. E-mail: lahiri@chem.iitb.ac.in*
[b]*Institut für Anorganische Chemie, Universität Stuttgart, Pfaffenwaldring 55, D-70550 Stuttgart, Germany. E-mail: kaim@iac.uni-stuttgart.de*
[c]*Department of Chemistry, Jadavpur University, Jadavpur, Kolkata-700032, India*
[d]*J. Heyrovský Institute of Physical Chemistry, v.v.i., Academy of Sciences of the Czech Republic, Dolejškova 3, CZ-18223 Prague, Czech Republic*
[e]*Center for Materials Characterization, National Chemical Laboratory, Dr. Homi Bhabha Road, Pune – 411008, India*

†Electronic supplementary information (ESI) available. CCDC 861089 (**1**), 861090 (**2**), 861091 (**3**), 861092(**4**), 861093 (**5**). For ESI and crystallographic data in CIF or other electronic format see DOI: 10.1039/c2dt31763j

In this context, the potential of the bis-tridentate, redox non-innocent, and inherently non-planar bridging ligand 2,3,5,6-tetrakis(2-pyridyl)pyrazine (tppz) for electron-transfer mediation between ruthenium termini containing a variety of ancillary ligands (L, X) (**B**) with different electronic properties has been studied in recent years (Table S1†).[7] The low-lying empty π*-orbital of the central pyrazine ring of coordinated bridging tppz has been established as an efficient mediator for intramolecular inter-metallic electron-transfer processes. The robust [Ru(μ-tppz)-Ru]^n platform has also been utilised recently in fabricating extended molecular frameworks.[7p,q]

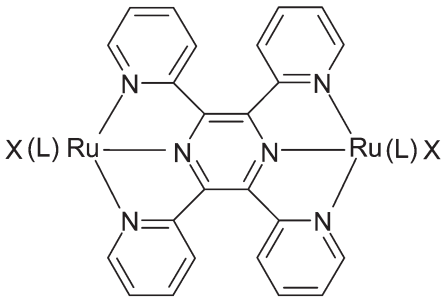

B

The complexes studied so far have shown appreciable variations in the comproportionation constant, K_c ($RT\ln K_c = nF(\Delta E)$); depending on the ancillary ligands in **B** (Table S1†). K_c is a thermodynamic parameter that reflects the stability of an intermediate state with respect to disproportionation to the adjacent redox states. Whilst some stabilisation may be due to 'resonance' (delocalisation), other factors unrelated to the electronic structure of the complex can also influence K_c.[4d] The significance of K_c for practical purposes, especially for isolability of the intermediate, is obvious. Complexes with bidentate (L) and monodentate (X = Cl) ligands at the ruthenium termini were shown to exhibit K_c values of 10^3–10^7, depending on the acceptor or donor nature of L (Table S1†). Spectroelectrochemical studies (UV-Vis-NIR-IR, EPR) in combination with DFT calculations have suggested valence-delocalised (class III according to Robin and Day[8]) or borderline class II–III mixed-valent $Ru^{II}Ru^{III}$ situations.[7d–j,l,m,o]

The present article describes a systematic study of tppz-bridged diruthenium complexes [Cl(L)Ru(μ-tppz)Ru(L)Cl] (**1–5**, Scheme 1), incorporating electron-rich bidentate β-diketonates as ancillary ligands. β-diketonato complexes have found a wide range of applications due to their stability, variability, and shielding properties.[9] We can report a significant enhancement of K_c to 10^{10}–10^{12} for $\mathbf{1}^+$–$\mathbf{5}^+$ in relation to the K_c values reported for analogous complexes (Table S1†).[7d–j,l,m,o] The systems $\mathbf{1}^+$–$\mathbf{5}^+$ also exhibit notable variations in K_c, depending on the electronic nature of L and on the configuration, *syn* or *anti*, of the complexes (Scheme 1).

Herein we describe the syntheses, molecular structures and (spectro)electrochemistry (UV-Vis-NIR, EPR) of the diruthenium(II) complexes **1–5**. Compound **4** was found to be converted to a Cl^-/CH_3CN exchanged product on single crystal formation. The electronic properties of the redox series $\mathbf{1}^n$–$\mathbf{5}^n$ (n = 2+ to −) will be analysed in relation to those of related complexes by

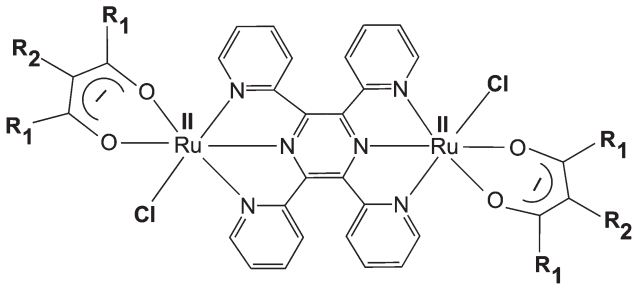

anti configuration

		Complex
$R_1 = CH_3$	$R_2 = H$	1
$R_1 = C_2H_5$	$R_2 = H$	2
$R_1 = CH_3$	$R_2 = CH_3$	4
$R_1 = CH_3$	$R_2 = C_2H_5$	5

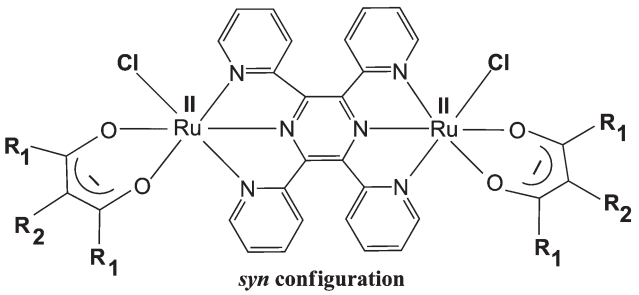

syn configuration

		Complex
$R_1 = {}^tBu$	$R_2 = H$	3

Scheme 1

experimental studies (UV-Vis-NIR, EPR spectroscopy) and DFT calculations.

Results and discussion

Synthesis and structures

Complexes [Cl(L)Ru^{II}(μ-tppz)Ru^{II}(L)Cl] (**1–5**, Scheme 1) were prepared from [Cl_3Ru(μ-tppz)$RuCl_3$] and the corresponding β-diketones. Microanalytical data, mass and ^{1}H NMR spectroscopy confirm the identity of the products (Fig. S1, S2† and Experimental section). Single crystals of compounds **1–3** and **5** have been obtained and their molecular structures were determined (Fig. 1–4). The product from the crystallisation of **4** in CH_3CN was shown to be a chloride/acetonitrile substitution form [$(CH_3CN)(L)Ru^{II}$(μ-tppz)$Ru^{II}(L)(CH_3CN)](Cl)_2 \cdot 4H_2O$, L = 3-methyl-2,4-pentanedionato (Tables S2, S3 and Fig. S3†). The crystallographic and selected bond parameters for **1**, **2**, **3** and **5** are listed in Tables 1, 2 and S4,† respectively. The calculated bond parameters based on the DFT optimised structures of the representative systems **1** and **3** (Table 3 and Fig. S4†) match well with the corresponding experimental values (Tables 2 and S4†). Compounds **1–5** can exist in *anti* and *syn* configurations with respect to the two monodentate ligands (Scheme 1). In all cases only one isomer has been isolated.

Crystal structure analysis establishes the selective formation of the *anti* configuration in **1**, **2**, **5** and in the Cl^-/CH_3CN

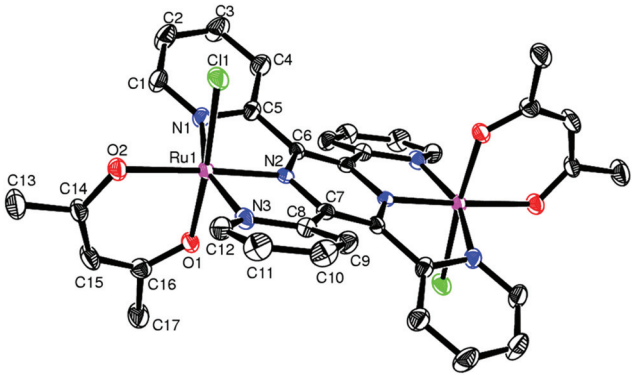

Fig. 1 Oak Ridge Thermal Ellipsoid Plot (ORTEP) diagram of **1**. Ellipsoids are drawn at 50% probability level. Hydrogen atoms are omitted for clarity.

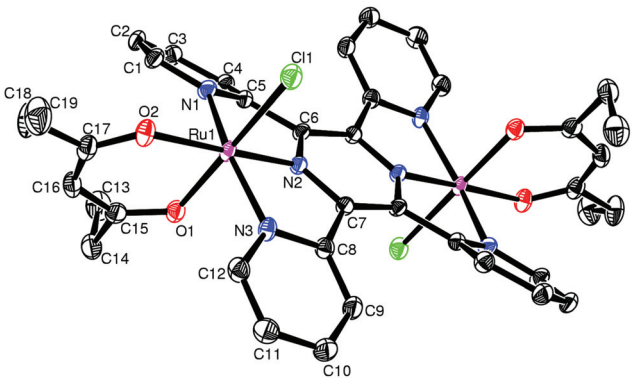

Fig. 2 ORTEP diagram of **2**. Ellipsoids are drawn at 50% probability level. Hydrogen atoms are omitted for clarity.

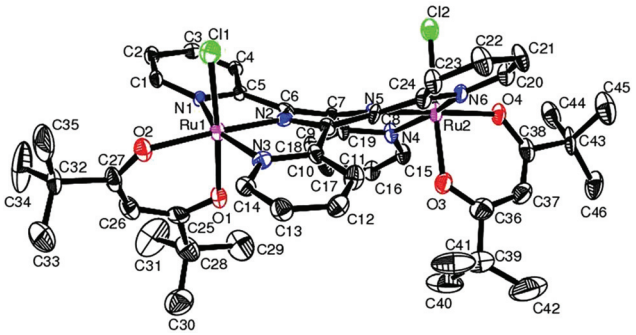

Fig. 3 ORTEP diagram of **3**. Ellipsoids are drawn at 50% probability level. Hydrogens and disordered atoms are removed for clarity.

exchanged species $[(CH_3CN)(L)Ru^{II}(\mu\text{-tppz})Ru^{II}(L)(CH_3CN)](Cl)_2{\cdot}4H_2O$ (**4′**) whereas compound **3** was isolated and characterised as the *syn* isomer. We suggest that the effect of bulky ^{t}Bu groups in the terminal β-diketone ligand of **3** causes the stabilisation of the *syn* configuration. The angles, ClRuRu′Cl′ or $(CH_3CN)RuRu'(NCCH_3)'$ in **1**, **2**, **4′**, **5** (*anti*) and **3** (*syn*) are 180°, 180°, 149.30°, 155.9° and 43.2°, respectively. The chelate bite angles and the *trans*-angles (E–Ru–E′, E/E′ = N, O, Cl) in the complexes are in the range of 79.57°–101.33° and 158.99°–

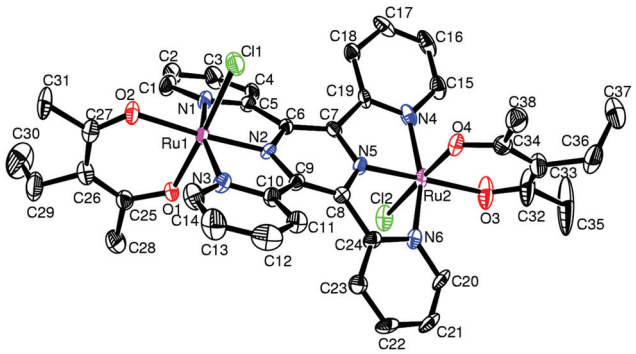

Fig. 4 ORTEP diagram of **5**. Ellipsoids are drawn at 50% probability level. Hydrogen atoms and solvents of crystallisation are removed for clarity.

179.5°, respectively, which essentially reflects distorted octahedral environments around the ruthenium centres. The interligand *trans*-angles involving terminal β-diketonates, bridging tppz and monodentate Cl^- or CH_3CN, are close to 180° (>175°). However, steric constraints, due to the meridionally coordinated non-planar tppz ligand, introduce smaller intraligand *trans*-angles (N1–Ru1–N3/N4–Ru2–N6) of close to 160°.[7d,f,l,m,o] The dihedral angles between the two pyridine rings of tppz in **1**–**3**, **4′** and **5** are 43.0°, 40.1°, 12.7°/22.8°, 6.0° and 8.7°/13.1°, respectively. The dihedral angles between the pyridine rings and the central pyrazine ring of tppz are 22.6°/22.9°, 21.9°/19.1°, 26.5°/24.0°/34.2°/26.1°, 24.8°/22.0° and 26.0°/17.3°/26.0°/26.9° for **1**–**3**, **4′** and **5**, respectively. In **1** and **2** the central pyrazine ring of the bridging tppz ligand is planar, however, in **3**, **4′** and **5**, the pyrazine rings are slightly non-planar, despite their aromatic character,[7l] and the deviations from planarity are estimated by the folding angles (N2C6C7N5/N2C9C8N5 or N2C6C′6N′2/N2C7C′7N′2) as 4.51°, 3.83° and 3.78°, respectively (Fig. S5†). Consequently, the two planes involving Ru1N1N2N3 and Ru′1N′1N′2′N3 in symmetric **1** and **2** are parallel, whereas the dihedral angles between the two planes, Ru1N1N2N3 and Ru2N4N5N6 in **3**, **5** and RuN1N2N3 and Ru′N′1N′2′N3 in **4′**, are 40.4°, 26.0° and 27.9°, respectively.

The Ru–N(pyrazine, tppz) distances of 1.905(5) Å–1.918(6) Å are significantly shorter than the corresponding Ru–N(pyridine)(tppz) distances, 2.018(5) Å–2.067(6) Å, due to the (dπ) Ru^{II} → (pπ*)pyrazine(tppz) back-bonding effect which facilitates the strong intermetallic electronic coupling in the mixed-valent $Ru^{II}Ru^{III}$ state (see later).[7d,f,l,m,n,o] The Ru–N(pyrazine, tppz) distances in **1**–**3**, **4′** and **5** (≤1.918(6) Å) are appreciably shorter than those reported in analogous tppz-bridged diruthenium(II) complexes $[Cl(L)Ru^{II}(\mu\text{-tppz})Ru^{II}(L)Cl]^{2+}$ with π-acidic ancillary ligands, L = 4,4′-dimethy-2,2′-bipyridine (1.944(3)/1.955(3) Å)[7d] or L = 2-phenylazopyridine (1.965(9)/1.941(8)/1.957(10) Å),[7f] or in $[Cl(bpy)Ru^{II}(\mu\text{-tppz})Ru^{III}(tpy)]^{3+}$ (1.932(4)/1.963(4) Å) (tpy = 2,2′:6′,2″-terpyridine).[7t] However, they are comparable with the values for the complexes $[Cl(L)Ru^{II}(\mu\text{-tppz})Ru^{II}(L)Cl]$ containing anionic ancillary ligands such as L = 2-picolinato (1.930 Å),[7l] 2-quinolinecarboxylato (1.901 Å),[7l] 8-quinolinecarboxylato (1.937 Å),[7l] or 3,5-di-*tert*-butyl-*o*-benzosemiquinone (1.921 Å).[7m] The effect of electron-rich σ/π-donating β-diketonato ligands in **1**–**5** strengthens the metal-to-tppz back-

Table 1 Crystallographic data and refinement parameters for **1–3** and **5**

	1	**2**	**3**	**5**·CH_2Cl_2 ·C_2H_5OH·$2H_2O$
Empirical formula	$C_{34}H_{30}Cl_2N_6O_4Ru_2$	$C_{38}H_{38}Cl_2N_6O_4Ru_2$	$C_{46}H_{54}Cl_2N_6O_4Ru_2$	$C_{41}H_{50}Cl_4N_6O_7Ru_2$
Formula weight	859.68	915.78	1027.99	1082.81
Crystal size (mm)	0.28 × 0.23 × 0.21	0.33 × 0.27 × 0.21	0.32 × 0.28 × 0.22	0.28 × 0.23 × 0.18
Crystal system	Monoclinic	Triclinic	Triclinic	Triclinic
Space group	$P2_1/c$	$P\bar{1}$	$P\bar{1}$	$P\bar{1}$
a (Å)	12.2324(3)	8.8953(2)	12.1020(3)	12.810(1)
b (Å)	8.4934(2)	9.2556(2)	13.1171(4)	13.387(1)
c (Å)	15.8447(5)	11.3444(3)	15.5789(4)	14.811(1)
α (°)	90	101.726(2)	77.721(3)	107.566(7)
β (°)	94.136(3)	99.723(2)	87.363(2)	95.731(6)
γ (°)	90	98.659(2)	75.475(2)	106.692(7)
V (Å^3)	1641.89(8)	884.68(4)	2339.17(11)	2270.6(3)
Z	2	1	2	2
ρ_{calcd} (g cm^{-3})	1.739	1.719	1.460	1.584
μ (mm^{-1})	1.132	1.056	0.808	0.955
T (K)	150(2)	150(2)	150(2)	150(2)
hkl range	−14 to 14, −10 to 9, −18 to 18	−10 to 10, −10 to 10, −13 to 13	−14 to 14, −15 to 15, −18 to 18	−15 to 8, −15 to 15, −16 to 17
F(000)	860	462	1052	1100
θ range (°)	3.24 to 25.00	3.28 to 25.00	3.31 to 25.00	3.29 to 25.00
Reflns collected	11 933	6381	16 836	17 236
Unique reflns (R_{int})	2887 [0.0480]	3103 [0.0235]	8234 [0.0646]	7978 [0.0435]
Data/restraints/ parameters	2887/0/219	3103/0/237	8234/66/584	7978/12/565
R_1, wR_2 ($I > 2\sigma(I)$)	0.0293, 0.0628	0.0247, 0.0592	0.0435, 0.0639	0.0564, 0.1430
R_1, wR_2 (all data)	0.0432, 0.0648	0.0294, 0.0601	0.0936, 0.0700	0.0861, 0.1533
GOF	0.941	1.038	0.745	1.033
Largest diff. peak/hole (e Å^{-3})	0.471/−0.336	0.583/−0.325	0.559/−0.543	1.476/−1.229

Table 2 Selected bond lengths (Å) for **1–3** and **5**

Bond lengths	**1**	**2**	**3**	**5**
Ru1–N2	1.918(3)	1.909(2)	1.907(4)	1.918(5)
Ru1–N1	2.032(3)	2.045(2)	2.030(4)	2.041(5)
Ru1–N3	2.053(3)	2.025(2)	2.040(4)	2.047(5)
Ru1–O1	2.053(2)	2.050(2)	2.050(4)	2.034(4)
Ru1–O2	2.066(2)	2.092(2)	2.069(3)	2.055(4)
Ru1–Cl1	2.370(1)	2.382(1)	2.365(1)	2.383(2)
Ru2–N5			1.912(4)	1.905(5)
Ru2–N4			2.030(4)	2.034(5)
Ru2–N6			2.025(4)	2.018(5)
Ru2–O3			2.016(4)	2.054(4)
Ru2–O4			2.056(3)	2.032(5)
Ru2–Cl2			2.382(1)	2.399(2)

Table 3 Selected experimental and DFT-calculated bond lengths (Å) for $\mathbf{1}^n$ and $\mathbf{3}^n$

	1		$\mathbf{1}^+$	$\mathbf{1}^{2+}$
Bonds	X-ray	DFT	DFT	DFT
Ru1–N1	2.032(3)	2.068	2.086	2.094
Ru1–N2	1.918(3)	1.944	1.946	1.965
Ru1–N3	2.053(3)	2.069	2.085	2.098
Ru1–O1	2.053(2)	2.086	2.074	2.016
Ru1–O2	2.066(2)	2.104	2.069	2.062
Ru1–Cl1	2.370(1)	2.414	2.356	2.340
	3		$\mathbf{3}^+$	$\mathbf{3}^{2+}$
Ru1–N1	2.030(4)	2.071	2.052	2.113
Ru1–N2	1.907(4)	1.940	1.922	1.983
Ru1–N3	2.040(4)	2.062	2.056	2.067
Ru1–O1	2.050(4)	2.086	2.063	2.023
Ru1–O2	2.069(3)	2.103	2.075	2.056
Ru1–Cl1	2.365(1)	2.404	2.365	2.341
Ru2–N4	2.030(4)	2.064	2.050	2.078
Ru2–N5	1.912(4)	1.940	1.923	1.974
Ru2–N6	2.025(4)	2.071	2.049	2.112
Ru2–O3	2.016(4)	2.088	2.035	2.021
Ru2–O4	2.056(3)	2.100	2.063	2.055
Ru2–Cl2	2.382(1)	2.403	2.377	2.346

bonding and the intermetallic electronic coupling in the $Ru^{II}Ru^{III}$ states of $\mathbf{1}^+$–$\mathbf{5}^+$ (see later). As will be further discussed below, the slightly smaller Ru···Ru separation of 6.487 Å in the *syn* complex (**3**) with respect to the *anti* complexes [**1** (6.526 Å), **2** (6.520 Å), **4**′ (6.523 Å) and **5** (6.507 Å)], as well as the greater donor effect from the ^{t}Bu groups in the β-diketonato functions, is believed to contribute to the 100 fold greater electrochemical coupling (comproportionation constant $K_c = 10^{12}$) in the Ru^{II}-Ru^{III} state of $\mathbf{3}^+$, as compared to that of the *anti* complexes ($\mathbf{1}^+$, $\mathbf{2}^+$, $\mathbf{4}^+$, $\mathbf{5}^+$, $K_c \sim 10^{10}$) (see later, Table 4). The average Cl···Cl separation in the *anti* complexes (**1**, **2**, **5**) of about 8.157 Å is expectedly larger than that in the *syn* complex **3** with 7.538 Å. The Cl···Cl distance in the *anti* complexes matches well with values for other such systems.[7f,l,m,o] However, the Cl···Cl distance of 7.538 Å in the *syn* complex (**3**) is significantly longer than the values reported for two other *syn* complexes [Cl(L)Ru^{II}(μ-tppz)-Ru^{II}(L)Cl] with L = 2-quinolinecarboxylato (5.710 Å)[7l] and [Cl(L)Ru^{II}(μ-tppz)Ru^{II}(L)Cl]$^{2+}$ with L = 4,4′-dimethy-2,2′-bipyridine (5.880 Å).[7d] This difference is the result of almost linear *trans* angles, O1–Ru1–Cl1, 176.07(10)° and O3–Ru2–Cl2, 177.46(10)° in **3**. The average Ru^{II}–Cl (2.380 Å)[7d,f,l,m,o] and Ru^{II}–O (2.051 Å)[10] bond lengths correspond to standard values;

Table 4 Electrochemical data[a]

	$E°_{298}$/V (ΔE_p/mV)[b]							
Complex	Ox1	Ox2	ΔE (V)	Red1	Red2	ΔE (V)	K_{c1}[c] between Ox1 and Ox2	K_{c2} between Red1 and Red2
1	0.17(80)	0.76(70)	0.59	−1.00(90)	−1.54(90)	0.54	10^{10}	1.4×10^9
2	0.16(80)	0.76(80)	0.60	−1.01(90)	−1.57(100)	0.56	1.5×10^{10}	3.1×10^9
3	0.14(90)	0.85(90)	0.71	−1.01(90)	−1.55(90)	0.54	1.1×10^{12}	1.4×10^9
4	0.10(90)	0.69(90)	0.59	−1.01(70)	−1.56(90)	0.55	10^{10}	2.1×10^9
5	0.09(90)	0.69(80)	0.60	−1.03(80)	−1.56(90)	0.53	1.5×10^{10}	9.6×10^8

[a] From cyclic voltammetry in CH_3CN/0.1 mol dm^{-3} Et_4NClO_4 at 100 mV s^{-1}. [b] In V *versus* SCE; peak potential differences ΔE_p (mV) (in parentheses). [c] Comproportionation constant from $RT\ln K_c = nF(\Delta E)$.

the Ru–O bond lengths *trans* to the π-accepting pyrazine ring of tppz are 0.013–0.042 Å longer than those *trans* to the π-donating chloride ligand.

The DFT geometry optimisations which have well reproduced the experimental structures of neutral **1** and **3** have been extended to the cation and dication species $\mathbf{1}^+$, $\mathbf{1}^{2+}$, $\mathbf{3}^+$, and $\mathbf{3}^{2+}$. As Table 3 reveals, metal-based oxidations (*cf.* below) result in the expected shortening of the more ionic Ru–O and Ru–Cl bonds. In contrast, the Ru–N bond lengths to π-accepting tppz increase on going from *anti*-configured **1** *via* $\mathbf{1}^+$ to $\mathbf{1}^{2+}$, reflecting diminished π-back-bonding along that series. However, the *syn*-configured system $\mathbf{3}^{n+}$ shows a different pattern, with a minimum Ru–N bond length for the monocationic mixed-valent intermediate $\mathbf{3}^+$ (Table 3). This remarkable DFT result is in agreement with the special stabilisation of that ion, as experimentally proven by its particularly high K_c value of 10^{12} (Table 4).

Electrochemistry and EPR spectroscopy

The complexes **1–5** exhibit two one-electron reversible successive oxidation and two successive one-electron reduction processes within the experimental potential range of ±2.0 V *versus* SCE in CH_3CN/0.1 mol dm^{-3} Et_4NClO_4. Redox potentials are listed in Table 4 and the voltammograms are shown in Fig. 5. In the absence of easily oxidisable ligands, the oxidations are believed to be associated with metal-based processes: $Ru^{II}Ru^{II} \rightleftharpoons Ru^{II}Ru^{III}$ (Ox1) and $Ru^{II}Ru^{III} \rightleftharpoons Ru^{III}Ru^{III}$ (Ox2) (Fig. 5). Accordingly, the DFT calculated HOMO/HOMO − 1 orbitals of the representative compounds **1** and **3**, as well as the singly occupied MO (SOMO) of one-electron oxidised $\mathbf{1}^+$ or $\mathbf{3}^+$, are dominated by ruthenium-based orbitals (Tables S5–S8 and Fig. S6–S9†).

Support for this assignment comes from EPR spectroscopy: after one-electron oxidation the $Ru^{II}Ru^{III}$ states in $\mathbf{1}^+$–$\mathbf{5}^+$ exhibit $Ru^{III}(t_{2g}^5)$ type anisotropic EPR signals with $\langle g \rangle$ ($\langle g \rangle = [1/3(g_1^2 + g_2^2 + g_3^2)]^{1/2}$)[11] and Δg ($\Delta g = g_1 - g_3$) of 2.304–2.234 and 0.99–0.82, respectively, at 110 K in CH_3CN (Table 5 and Fig. 6a, S10†). The slight variations of $\langle g \rangle$ as well as of Δg in the EPR spectra of $\mathbf{1}^+$–$\mathbf{5}^+$ can be attributed to substituent effects of the β-diketonate ligands (Scheme 1). Spin-density plots and Mulliken spin distribution values for $\mathbf{1}^+$ and $\mathbf{3}^+$ reveal that the metal ions are the primary spin-bearing centres (Fig. 7a, S11a† and Table 6). The almost equal spin distribution calculated for the ruthenium ions in $\mathbf{1}^+$ or $\mathbf{3}^+$ suggests a delocalised mixed-

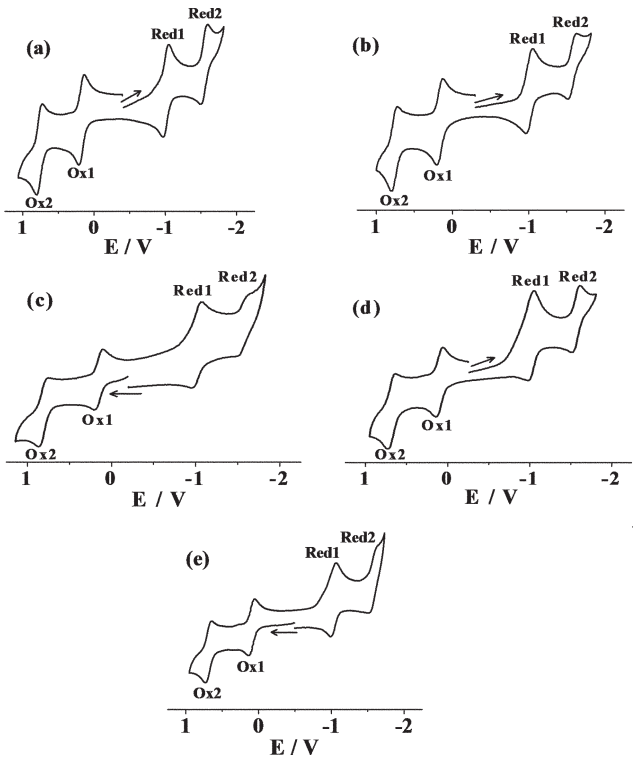

Fig. 5 Cyclic voltammograms of (a) **1**, (b) **2**, (c) **3**, (d) **4** and (e) **5** in CH_3CN, 0.1 mol dm^{-3} NEt_4ClO_4 at 298 K. Scan rate: 100 mV s^{-1}.

Table 5 EPR data[a] of $\mathbf{1}^n$–$\mathbf{5}^n$

Complex	g_1	g_2	g_3	$\langle g \rangle$	Δg
$\mathbf{1}^+$	2.77	2.23	1.81	2.304	0.96
$\mathbf{2}^+$	2.76	2.23	1.77	2.289	0.99
$\mathbf{3}^+$	2.65	2.25	1.83	2.268	0.82
$\mathbf{4}^+$	2.63	2.25	1.73	2.234	0.90
$\mathbf{5}^+$	2.65	2.24	1.81	2.259	0.84
	$g_{\parallel}$	$g_{\perp}$		$\langle g \rangle$	Δg
$\mathbf{1}^-$	2.010	1.994		2.005	0.016
$\mathbf{2}^-$	2.007	1.992		2.002	0.015
$\mathbf{3}^-$	2.011	1.998		2.007	0.013
$\mathbf{5}^-$	2.007	1.995		2.003	0.012

[a] From *in situ* measurements at 110 K in CH_3CN, 0.1 mol dm^{-3} Bu_4NPF_6; electrolytic oxidation and reduction, respectively.

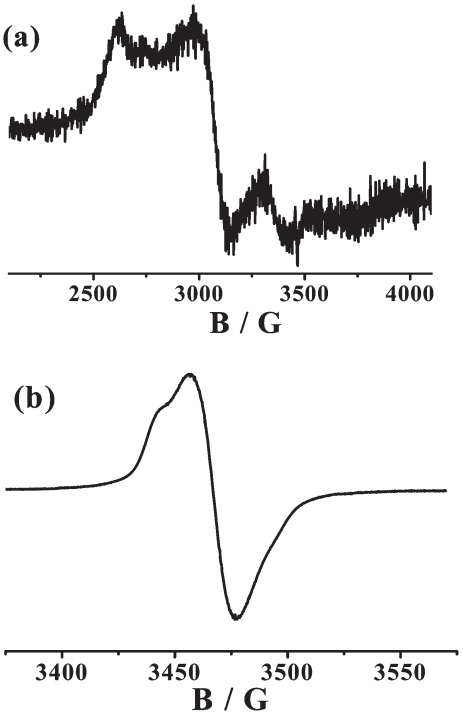

Fig. 6 EPR spectra of (a) $\mathbf{3}^{+}$ and (b) $\mathbf{3}^{-}$ in CH_3CN, 0.1 mol dm^{-3} Bu_4NPF_6 at 110 K.

valent situation, as supported by the high K_c values of 10^{10}–10^{12} (Table 4). The *g* anisotropies in $\mathbf{1}^{+}$–$\mathbf{5}^{+}$ (Δg: 0.99–0.82, Table 5) are smaller than that reported for the Creutz–Taube ion (Δg = 1.445),[12] which implies the participation of the bridging and unsaturated ancillary ligands in the spin accommodation.

The first oxidation (Ox1) potential decreases slightly with increasing +*I*-effect of the substituents, Me < Et < ^{t}Bu, in the $acac^{-}$-type ligands of **1**, **2**, and **3**, respectively, accompanied by the smaller HOMO–LUMO energy separation of **3** (1.68 eV) as compared to that of **1** (1.87 eV) (Fig. 8). The decrease of the first oxidation potential is more pronounced in **4** and **5** where the –CH proton of $acac^{-}$ has been substituted by electron-donating Me or Et groups. The first oxidation potentials of 0.09–0.17 V *versus* SCE for **1**–**5** (Table 4) are considerably lower than those reported for analogous complexes $[Cl(L)Ru^{II}(\mu\text{-tppz})Ru^{II}(L)Cl]^{2+}$ with neutral ligands, L = 2-phenylazopyridine (1.28 V),[7f] 2,2′-bipyridine (0.96 V),[7d] 2-(2-pyridyl)benzthiazole (0.95),[7h] 2-(2-pyridyl)benzoxazole (0.92),[7h] 2,2′-dipyridylketone (0.84 V),[7i] 2,2′-dipyridylamine (0.68 V),[7g] and 1-methyl-2-(2-pyridyl)-1*H*-benzimidazole (0.78 V)[7h] or with anionic ancillary ligands L = 2-(2-pyridyl)benzimidazolate (0.43 V),[7h] 2-picolinate (0.36 V),[7l] 2-quinolinecarboxylate (0.47 V),[7l] and 8-quinolinecarboxylate (0.31 V).[7l] The superior electron-donating ability of the β-diketonates increases the electron density on the metal ions, which results in stronger intermetallic electronic coupling between the π-acceptor-bridged mixed valent states in $\mathbf{1}^{+}$–$\mathbf{5}^{+}$ (electron transfer mechanism of valence exchange[2a]).

The potential separation of 0.59–0.71 V between the successive oxidation processes (Ox2–Ox1) of **1**–**5** leads to rather high comproportionation constants, $K_c \geq 10^{10}$ (Table 4). This order of magnitude implies substantial thermodynamic stability of the

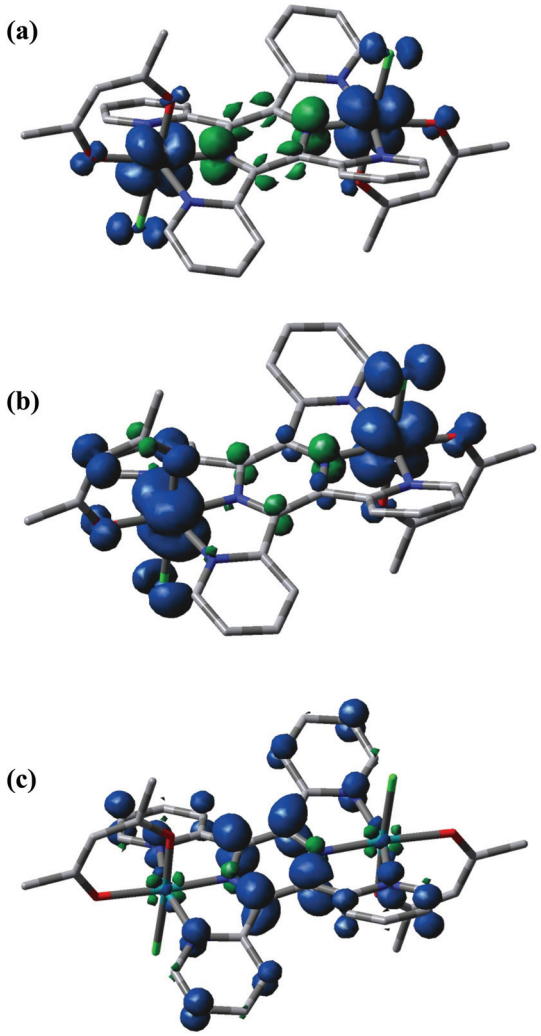

Fig. 7 Spin density plots of (a) $\mathbf{1}^{+}$, (b) $\mathbf{1}^{2+}$ and (c) $\mathbf{1}^{-}$.

Table 6 Spin densities of complexes calculated from DFT

Complex	Ru1	Ru2	tppz	L	Cl1	Cl2
$\mathbf{1}^{+}$	0.6198	0.6190	−0.4086	0.0312	0.0697	0.0689
$\mathbf{1}^{2+}$	0.7578	0.8496	−0.0125	0.1412	0.1498	0.1141
$\mathbf{1}^{-}$	−0.0035	−0.0035	0.9902	0.0016	−0.0022	−0.0022
$\mathbf{3}^{+}$	0.6057	0.5932	−0.3681	0.0432	0.0643	0.0617
$\mathbf{3}^{2+}$	0.7312	0.7605	−0.0215	0.3084	0.1160	0.1054
$\mathbf{3}^{-}$	0.0197	0.0003	0.9748	0.0085	−0.0017	−0.0016

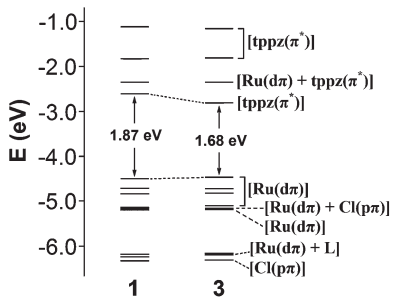

Fig. 8 Orbital energy diagrams for **1** and **3**.

mixed-valent state as anticipated for a valence-delocalised class III mixed-valence situation according to the Robin and Day definition.[8] The K_c value varies depending on the β-diketonate terminal ligands to some extent, following the order $\mathbf{1}^+ \sim \mathbf{4}^+ < \mathbf{2}^+ \sim \mathbf{5}^+ < \mathbf{3}^+$. The high K_c value of 10^{12} for complex **3** can be attributed both to the strong +*I*-effect of ^{t}Bu group and to the sterically enforced *syn* configuration with rather upright Ru–Cl vectors and linear *trans* angles O–Ru–Cl. The present set of tppz-bridged complexes **1–5** thus exhibits remarkably high K_c values of $\geq 10^{10}$ (Table 4) in contrast to several related complexes $[Cl(L)Ru^{II}(\mu\text{-tppz})Ru^{II}(L)Cl]^{2+/0}$ with K_c of 10^3–10^7 (Table S1†).[7d–j,l,m]

The splitting of oxidation potentials for $\mathbf{1}^+$–$\mathbf{5}^+$ is almost double that reported for $[(NH_3)_5Ru^{II}(\mu\text{-pz})Ru^{III}(NH_3)_5]^{5+}$ ($\Delta E \approx 0.35$ V, $K_c \approx 10^6$, pz = pyrazine).[1b] The role of the anionic donor ligands is also illustrated by comparing $[(NH_3)_3Ru^{II}(\mu\text{-tppz})Ru^{III}(NH_3)_3]^{5+}$ ($K_c \approx 10^8$)[7a] with $[Cl_3Ru^{II}(\mu\text{-tppz})Ru^{III}Cl_3]^-$ ($K_c \approx 10^{12}$).[7n]

Further one-electron oxidation (Ox2, Fig. 5) of the cations generates isovalent diruthenium(III) species, $[Cl(L)Ru^{III}(\mu\text{-tppz})Ru^{III}(L)Cl]^{2+}$ ($\mathbf{1}^{2+}$–$\mathbf{5}^{2+}$). DFT calculations on the optimised structure of $\mathbf{1}^{2+}$ and $\mathbf{3}^{2+}$ confirm that the energy of the triplet ($S = 1$) states are appreciably lower than those of the singlet ($S = 0$) states by 4707 cm^{-1} and 5327 cm^{-1}, respectively, as has been similarly observed in related ligand bridged diruthenium(III) complexes.[13] The spin-density plots of $\mathbf{1}^{2+}$ and $\mathbf{3}^{2+}$ (Tables 6 and S9–S10† and Fig. 7b, S11b†) reveal the metal ions as the primary spin bearing sites, with minor contributions from the peripheral ligands.

DFT calculations predict tppz dominated LUMO and LUMO + 1 orbitals in the representative complexes **1** and **3** (Tables S5–S6, S11–S12† and Fig. S6–S7, S12–S13†), suggesting that the successive two reductions of **1–5** (Fig. 5 and Table 4) essentially correspond to tppz ⇌ $tppz^{\cdot-}$ (Red1) and $tppz^{\cdot-}$ ⇌ $tppz^{2-}$ (Red2) processes.[7] The K_c values, calculated from the potential separation of Red1 and Red2 are in the order of 10^{10} (Table 4) which signifies appreciable thermodynamic stability of the $tppz^{\cdot-}$ radical bridged diruthenium(II) intermediate of $[Cl(L)Ru^{II}(\mu\text{-}tppz^{\cdot-})Ru^{II}(L)Cl]^-$ in $\mathbf{1}^{\cdot-}$–$\mathbf{5}^{\cdot-}$. Consequently, one-electron reduced $\mathbf{1}^{\cdot-}$–$\mathbf{3}^{\cdot-}$ and $\mathbf{5}^{\cdot-}$ as obtained by in-situ electrolysis display radical type EPR spectra in CH_3CN at 110 K (Table 5 and Fig. 6b and S14†).

The $\langle g \rangle$ (close to 2) and the small Δg values of 2.002–2.007 and 0.012–0.016, respectively (Table 5), prove the ligand centred spin. The Mulliken spin densities calculated for $\mathbf{1}^{\cdot-}$ and $\mathbf{3}^{\cdot-}$ (Fig. 7c and S11c,† Table 6) confirm the location of the unpaired electron at the tppz bridging ligand. No EPR signal has been detected for an electrolytically reduced solution of **4** even at 4 K, possibly due to exchange of labile chloride ligands (**4** → **4′**) and rapid EPR relaxation for the solvated complex formed. The distorted first reduction wave for compound **4** suggests electron transfer induced labilisation of the Ru–Cl bonds, as suggested by the earlier described Cl^-/CH_3CN exchange on crystallisation of **4**. As outlined above, the system $\mathbf{4}^n$ is also distinguished by EPR silence of the one-electron reduced form, which is assumed to have the anionic Cl^- ligand exchanged by neutral CH_3CN, leading to rapid relaxation and thus severe EPR line broadening of $[(CH_3CN)(L)Ru^{II}(tppz^{\cdot-})Ru^{II}(L)(CH_3CN)]^+$.

UV-Vis-NIR spectroelectrochemistry

The experimentally observed transitions in the complexes $\mathbf{1}^n$–$\mathbf{5}^n$ (n = 2+, +, 0, −) (Fig. 9 and Fig. S15–S18†) have been analysed through time-dependent density functional theory (TD-DFT) calculations of the representative systems $\mathbf{1}^n$ and $\mathbf{3}^n$ (Tables 7, 8 and S13†). The neutral precursor compounds **1–5** display weak absorptions ($\varepsilon \sim 1400$ dm^3 mol^{-1} cm^{-1}) in the NIR region between 1400–1000 nm in addition to strong bands in the Vis and UV regions. The wavelength of the NIR band varies in the order 1404 nm (**5**) > 1390 nm (**3**) > 1347 nm (**2**) > 1330 nm (**1**) > 1050 nm (**4**). Consequently, the calculated HOMO–LUMO energy gap of **3** (1.68 eV) is lower than that of **1** (1.87 eV) (Fig. 8). The bands in the NIR and visible regions are assigned

Table 7 UV-Vis-NIR spectroelectrochemical data for **1–5** in CH_3CN/0.1 mol dm^{-3} Bu_4NPF_6

Complex	λ_{max}/nm (ε/dm^3 mol^{-1} cm^{-1})
$\mathbf{1}^{2+}$	641(7900), 573(sh), 514(7100), 386(32 500), 369(32 000), 296(30 000), 269(28 400)
$\mathbf{1}^+$	1680(2900), 637(20 500), 475(sh), 385(sh), 362(32 000), 98(28 900), 264(29 000)
1	1330(1400), 1015(2100), 674(21 000), 495(sh), 390(sh), 355(35 700), 294(27 000), 262(31 500)
$\mathbf{1}^-$	1130(3900), 1024(5700), 670(13 500), 580(sh), 488(sh), 439(33 600), 391(31 800), 377(32 000), 324(27 000), 287(sh), 269(32 000)
$\mathbf{2}^{2+}$	654(9400), 505(7300), 387(30 700), 370(30 800), 298(28 000), 270(26 500)
$\mathbf{2}^+$	1688(3300), 636(23 600), 467(sh), 385(sh), 360(33 100), 300(28 600), 267(28 700)
2	1347(1700), 1017(2100), 676(23 000), 497(sh), 357(35 500), 295(27 400), 265(30 700)
$\mathbf{2}^-$	1140(4100), 1025(6200), 670(13 600), 597(13 200), 490(sh), 440(36 400), 384(33 000), 324(27 700), 285(sh), 270(34 100)
$\mathbf{3}^{2+}$	655(9100), 605(sh), 518(7200), 387(32 500), 370(33 400), 291(36 000), 275(sh)
$\mathbf{3}^+$	1750(3000), 639(21 000), 473(sh), 387(sh), 358(35 000), 291(32 500), 265(35 700)
3	1390(1400), 1060(1900), 688(19 500), 505(7800), 403(sh), 350(38 000), 300(31 000), 263(38 500)
$\mathbf{3}^-$	1177(3400), 1048(5200), 665(11 500), 594(12 300), 495(sh), 442(34 000), 380(32 400), 329(26 800), 285(sh), 265(37 400)
$\mathbf{4}^{2+}$	725(sh), 555(8300), 383(33 300), 367(33 100), 295(30 400), 267(26 800)
$\mathbf{4}^+$	1660(2300), 663(17 700), 385(sh), 363(33 900), 296(29 800), 266(28 800)
4	1050(sh), 665(18 200), 450(sh), 390(sh), 357(36 200), 295(29 100), 262(29 700)
$\mathbf{4}^-$	1168(4050), 1020(4700), 660(12 400), 583(12 900), 490(sh), 439(30 800), 390(29 200), 320(24 800), 294(25 600), 266(15 700)
$\mathbf{5}^{2+}$	736(8370), 542(7090), 381(32 580), 368(32 880), 295(32 580), 234(26 450)
$\mathbf{5}^+$	1674(2240), 638(19 080), 360(32 640), 297(29 800), 266(29 170), 238(23 660)
5	1404(1100), 1080(1480), 680(19 978), 515(sh), 350(36 510), 292(29 286), 262(29 147)
$\mathbf{5}^-$	1174(3720), 1037(5440), 675(11 360), 595(11 600), 440(33 560), 386(29 580), 326(25 600), 292(28 940), 267(27 570), 230(sh)

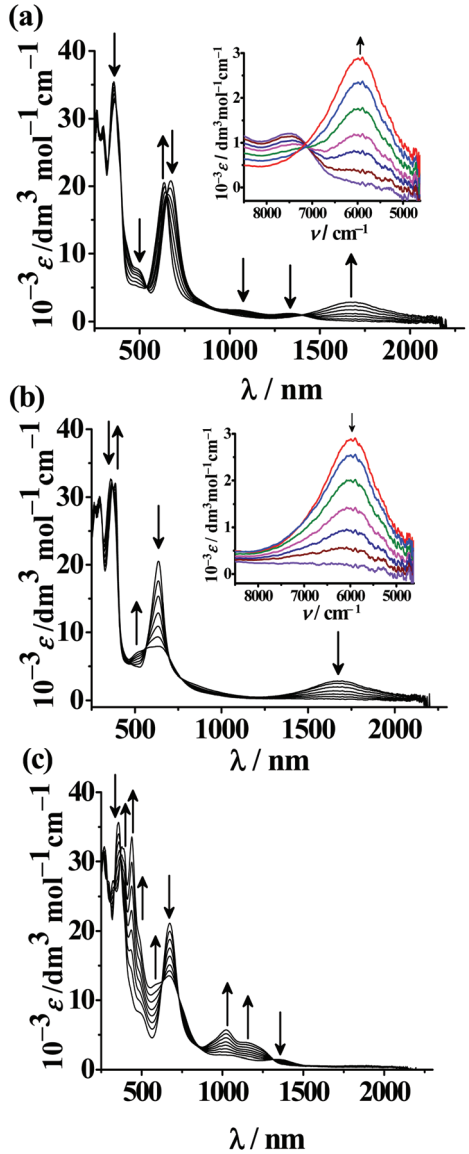

Fig. 9 UV-Vis-NIR spectroelectrochemistry for the conversions of (a) **1** → **1**$^+$, (b) **1**$^+$ → **1**$^{2+}$ and (c) **1** → **1**$^-$ in CH_3CN, 0.1 mol dm^{-3} Bu_4NPF_6 (inset shows the IVCT band in wave number scale).

according to TD-DFT calculations as Ru(dπ) → tppz(π*) (MLCT: metal-to-ligand charge-transfer), Ru(dπ) → tppz(π*)/Ru(dπ) (MLMCT: metal-to-ligand/metal charge-transfer) and Ru(dπ)/Cl(pπ) → tppz(π*) (MLLCT: metal/ligand-to-ligand charge-transfer) transitions.

After one-electron oxidation to the mixed-valent state in **1**$^+$–**5**$^+$, the weak NIR bands at about 1400–1000 nm disappear and the strong band near 700 nm shifts slightly to higher energy. Most conspicuously, the mixed-valent state in **1**$^+$–**5**$^+$ exhibits moderately strong ($\varepsilon \sim 2700$ dm^3 mol^{-1} cm^{-1}) MMCT absorptions in the NIR region with λ_{max} at 1750 nm (**3**$^+$) > 1688 nm (**2**$^+$) > 1680 nm (**1**$^+$) > 1674 nm (**5**$^+$) > 1660 nm (**4**$^+$). While the variation in energy is marginal for **1**$^+$, **2**$^+$, **4**$^+$ and **5**$^+$ with *anti* configuration, there is a more appreciable shift to lower energy for the *syn*-configured **3**$^+$. In accordance, the TD-DFT calculations on **1**$^+$ or **3**$^+$ predict metal-to-metal (Ru(dπ) → Ru(dπ)) transitions at 1810 and 1930 nm, respectively. The experimental band widths at half height ($\Delta\nu_{1/2}$) of the MMCT bands in **1**$^+$–**5**$^+$ are 1590, 1600, 1990, 2130 and 1840 cm^{-1}, respectively, and thus significantly lower than the respective calculated values of 3708, 3699, 3633, 3730 and 3714 cm^{-1}, based on the Hush formula, $\Delta\nu_{1/2} = (2310E_{op})^{1/2}$ (E_{op} = energy of the intervalence charge transfer (IVCT) band in cm^{-1})[3,5] for valence-trapped class II situations. This discrepancy clearly justifies the valence delocalised (class III[8]) mixed-valent ($Ru^{2.5}Ru^{2.5}$) description for **1**$^+$–**5**$^+$, as has been already inferred from the high K_c values of 10^{10}–10^{12} (Table 4). The calculated interaction energy (V_{AB}) values of **1**$^+$–**5**$^+$ at 2980, 2960, 2860, 3010, 2990 cm^{-1}, respectively, are then based on the assumption of a class III situation for which V_{AB} is considered as half the energy of the MMCT transition.[3b,7e,14] For comparison, the Creutz–Taube ion has 3185 cm^{-1} [7e], as determined by the same approach (Table S1†).

The MMCT band corresponding to the mixed-valent state completely disappears on oxidation of **1**$^+$–**5**$^+$ to the isovalent $Ru^{III}Ru^{III}$ forms in **1**$^{2+}$–**5**$^{2+}$. These triplet species exhibit mainly charge transfer bands in the visible region (Tables 7, 8 and S13†), involving the ligands (L, Cl, tppz) and metal-based orbitals.

The one-electron reduced ions **1**$^{\cdot-}$–**3**$^{\cdot-}$ and **5**$^{\cdot-}$ exhibit two new moderately intense bands at about 1200–1000 nm which are assigned based on previous observations[7l] and on TD-DFT calculations as mixed tppz(π) → tppz(π*) (SOMO → LUMO) intraligand transitions. In addition, several absorptions involving Ru(dπ)-to-tppz$^{\cdot-}$ transitions are observed in the visible region (Tables 7, 8 and S13†).

In fact, it is remarkable that potentially useful NIR absorbance[15] is observed here for the neutral species (weak MLCT transitions), for the mixed-valent monocationic intermediates (MMCT transitions), and for the one-electron reduced anion radical complexes (SOMO based intraligand transitions).

Conclusion

The incorporation of σ/π-donating β-diketonates L in the complex platform $[Cl(L)Ru(\mu\text{-tppz})Ru(L)Cl]^n$ [7d–j,l,m,o] enhances intramolecular metal-to-metal electronic interaction in the mixed-valent state (n = +1) through mediation by the π*-orbital of the tppz acceptor bridge. Large comproportionation constants K_c in the range of 10^{10}–10^{12} were observed for *anti* (**1**, **2**, **4**, **5**) and *syn* (**3**) configured complexes (Scheme 1, Table S1†). The mixed-valent states in **1**$^+$–**5**$^+$ exhibit metal-to-metal charge transfer absorptions around 1700 nm at moderate intensity ($\varepsilon \sim 2700$ dm^3 mol^{-1} cm^{-1}) and with relatively small bandwidth ($\Delta\nu_{1/2} \sim 1800$ cm^{-1}). A delocalised mixed-valent situation is thus inferred with V_{AB} at about 3000 cm^{-1}. The EPR-active cations (**1**$^+$–**3**$^+$ and **5**$^+$) show largely but not exclusively metal-centred spin, supported by calculated (**1**$^+$, **3**$^+$) spin densities on the metal ions (~0.6/Ru) and a sizeable (negative) spin density of about −0.4 on the tppz bridge, reflecting the electron transfer mechanism of valence exchange between metals *via* the π* MO of the bridge. While the spectroelectrochemically characterised **1**$^{2+}$–**5**$^{2+}$ were calculated with a triplet ground state, the reduced species **1**$^{\cdot-}$–**3**$^{\cdot-}$ and **5**$^{\cdot-}$ display radical type EPR signals and ligand based NIR transitions.[15]

Table 8 Electronic transitions at the TD-DFT/B3LYP/6-31G(d) level for $\mathbf{1}^n$ (n = 0, +, 2+, −)

$E_{excitation}$/eV	$\lambda_{excitation}$/nm (expt.)	Oscillator strength (expt.: ε/dm^3 mol^{-1} cm^{-1})	Transition	Character
1				
0.9563	1290 (1330)	0.0090 (1400)	(73%) HOMO → LUMO	Ru(dπ) → tppz(π*)
1.2477	993 (1015)	0.0262 (2100)	(76%) HOMO − 1 → LUMO	Ru(dπ) → tppz(π*)
1.8714	662 (674)	0.3861 (21 000)	(77%) HOMO − 1 → LUMO + 1	Ru(dπ) → tppz(π*)/Ru(dπ)
2.4843	500.1 (495)	0.1596	(87%) HOMO − 2 → LUMO + 2	Ru(dπ) → tppz(π*)
2.9837	410 (390)	0.0732	(56%) HOMO → LUMO + 4	Ru(dπ) → tppz(π*)
			(24%) HOMO − 5 → LUMO + 2	
3.1689	390	0.0214	(68%) HOMO − 6 → LUMO	L → tppz(π*)
3.3564	370	0.2165	(37%) HOMO − 7 → LUMO + 1	L → tppz(π*)
	(355)	(35 700)	(35%) HOMO − 12 → LUMO	tppz(π) → tppz(π*)
$\mathbf{1}^+$				
0.6832	1810 (1680)	0.0085 (2900)	(81%)HOMO − 3(β) → LUMO(β)	Ru(dπ) → Ru(dπ)
0.8444	1470	0.0396	(84%)HOMO(β) → LUMO(β)	Ru(dπ)/tppz(π) → Ru(dπ)
1.9696	630 (637)	0.0234 (20 500)	(86%)HOMO − 3(β) → LUMO + 1(β)	Ru(dπ) → tppz(π*)
2.0190	610	0.2388	(60%)SOMO1(α) → LUMO + 1(α)	Ru(dπ)/L → tppz(π*)
			(27%)HOMO − 2(α) → LUMO(α)	
2.5738	480 (475, 385)	0.0243	(95%)HOMO − 2(α) → LUMO + 1(α)	Ru(dπ)/Cl(pπ) → tppz(π*)
2.6373	470	0.0219	(50%)HOMO − 3(α) → LUMO + 1(α)	Ru(dπ)/Cl(pπ) → tppz(π*)
			(41%)HOMO − 9(β) → LUMO(β)	L/Cl(pπ) → Ru(dπ)
3.3392	370 (362)	0.2140 (32 000)	(71%)HOMO − 8(β) → LUMO + 1(β)	tppz(π) → tppz(π*)
$\mathbf{1}^{2+}$				
1.0549	1170	0.0117	(90%)HOMO(β) → LUMO(β)	Ru(dπ)/L → Ru(dπ)
1.6154	770	0.0143	(72%)SOMO1(α) → LUMO + 1(α)	Ru(dπ)/L → tppz(π*)
1.8990	650 (641)	0.0591 (7900)	(61%)HOMO − 1(β) → LUMO + 3(β)	Ru(dπ)/Cl(pπ) → tppz(π*)
1.9809	620	0.0489	(43%)SOMO2(α) → LUMO(α)	Ru(dπ)/Cl(pπ) → tppz(π*)
			(23%)HOMO − 1(β) → LUMO + 3(β)	
2.1284	580 (573)	0.0230	(71%)HOMO − 6(β) → LUMO(β)	L/Cl(pπ) → Ru(dπ)
2.1556	570	0.0147	(39%)HOMO − 6(β) → LUMO + 1(β)	L/Cl(pπ) → Ru(dπ)/tppz(π*)
			(36%)HOMO − 8(β) → LUMO(β)	
2.3890	520 (514)	0.0284 (7100)	(59%)HOMO − 8(β) → LUMO + 1(β)	L/Cl(pπ) → Ru(dπ)/tppz(π*)
2.4941	500	0.0270	(62%)HOMO − 7(β) → LUMO(β)	tppz(π) → Ru(dπ)
$\mathbf{1}^-$				
1.0656	1160 (1130)	0.0042 (3900)	(85%)SOMO(α) → LUMO(α)	tppz(π) → tppz(π*)
1.2244	1010	0.0136	(57%)SOMO(α) → LUMO + 1(α)	tppz(π) → tppz(π*)
	(1024)	(5700)	(23%)HOMO(β) → LUMO(β)	Ru(dπ) → tppz(π*)
1.7456	710 (670)	0.0711	(69%)SOMO(α) → LUMO + 2(α)	tppz(π) → tppz(π*)
		(13 500)	(22%)HOMO(β) → LUMO + 1(β)	Ru(dπ) → tppz(π*)
1.7956	690	0.0313	(63%)HOMO(β) → LUMO + 1(β)	Ru(dπ) → tppz(π*)
1.9270	640	0.0312	(63%)HOMO − 4(β) → LUMO(β)	Ru(dπ) → tppz(π*)
2.0353	610 (580)	0.1363	(64%)HOMO − 1(α) → LUMO + 1(α)	Ru(dπ) → tppz(π*)
2.4452	510	0.0233	(72%)HOMO − 4(α) → LUMO + 1(α)	Ru(dπ)/Cl(pπ) → tppz(π*)
2.4494	510	0.0567	(55%)HOMO − 2(β) → LUMO + 2(β)	Ru(dπ) → tppz(π*)
2.5173	490 (488)	0.0680	(61%)HOMO − 2(β) → LUMO + 3(β)	Ru(dπ) → tppz(π*)

Out of the five β-diketonato ligated systems $\mathbf{1}^n$–$\mathbf{5}^n$, the *anti*-configured compound **4** is distinguished by the lability of the Ru–Cl bonds as evident from crystallisation, cyclic voltammetry and (spectro)electrochemistry experiments. On the other hand, the redox system $\mathbf{3}^n$ is distinguished by the sterically induced preference for a *syn* configuration with rather upright Ru–Cl vectors, leading to an unusually high K_c of 10^{12} for $\mathbf{3}^+$, to a bathochromically shifted MMCT transition, and to DFT calculated minimum Ru–N bond lengths in comparison to the isovalent congeners **3** and $\mathbf{3}^{2+}$.

A formal similarity exists between the mixed-valent systems $\mathbf{1}^+$–$\mathbf{5}^+$ and [(tpy)Ru(μ-tpb-2H$^+$)Ru(tpy)]$^{3+}$, also involving a bis-tridentate bridge (tpy = 2,2′;6′,2″-terpyridine and tpb = 1,2,4,5-tetrakis(2-pyridyl)benzene).[11b] However, in contrast to the π-donating doubly deprotonated (tpb-2H$^+$) dicarbanion, the tppz acts as a neutral π-acceptor bridge, leading to an opposite valence transfer mechanism (electron *versus* hole transfer).[2a,4d] Characteristically, the [(A)Ru(μ-η^3:η^3-D)Ru(A)]$^{3+}$ ion (A = tpy acceptor; D = (tpb-2H$^+$) donor) and the systems [(D)ClRu-(μ-η^3:η^3-A)RuCl(D)]$^+$ described here (D = β-diketonato donor; A = tppz acceptor) produce different electrochemical and spectroscopic results. The lower energy (greater wavelength) and lower intensity of the IVCT transitions in $\mathbf{1}^+$–$\mathbf{5}^+$ illustrate that the electronic coupling is larger in the dicarbanion donor-bridged situation.[11b] However, in agreement with published concepts,[2a,4e] the acceptor-bridged systems $\mathbf{1}^+$–$\mathbf{5}^+$ are distinguished by larger K_c values ($10^{10} > 10^7$) and wider g anisotropy (g_1–g_3: $0.9 > 0.34$)[11b] because of the inherently[2a] small contribution from the bridge in the spin distribution of the singly occupied MO, leading to confinement of spin on the metals with their high spin–orbit coupling constant.

Experimental

Materials

The starting complex [Cl$_3$Ru(μ-tppz)RuCl$_3$] was prepared according to the reported procedure.[7d] The ligand acetylacetone

was obtained from Merck, India and other ligands, 3,5-heptanedione, 2,2,6,6-tetramethyl-3,5-heptanedione, 3-methyl-2,4-pentanedione and 3-ethyl-2,4-pentanedione were purchased from Aldrich, USA. Other chemicals and solvents were reagent grade and used as received. For spectroscopic and electrochemical studies, high performance liquid chromatography (HPLC) grade acetonitrile was used.

Physical measurements

UV-Vis-NIR spectroelectrochemical studies were performed in CH_3CN/0.1 M Bu_4NPF_6 at 298 K using an optically transparent thin layer electrode (OTTLE) cell[16] mounted in the sample compartment of a J&M TIDAS spectrophotometer. ^{1}H NMR spectra were obtained from 300 MHz Varian FT spectrometer and 400 MHz Bruker FT spectrometer. The EPR measurements were made in a two-electrode capillary tube[17] with an X-band Bruker system ESP300, equipped with a Bruker ER035M gaussmeter and a HP 5350B microwave counter. Cyclic voltammetric measurements were carried out using a PAR model 273A electrochemistry system. Platinum wire working and auxiliary electrodes and an aqueous saturated calomel reference electrode (SCE) were used in a three-electrode configuration. The supporting electrolyte was 0.1 mol dm^{-3} Et_4NClO_4 and the solute concentration was $\sim 10^{-3}$ mol dm^{-3}. The half-wave potential $E°_{298}$ was set equal to 0.5(E_{pa} + E_{pc}), where E_{pa} and E_{pc} are anodic and cathodic cyclic voltammetric peak potentials, respectively. Elemental analyses were carried out on a Perkin-Elmer 240C elemental analyser. Electrospray mass spectra were recorded on a Micromass Q-ToF mass spectrometer.

Preparation of complexes

Synthesis of 1–3. The complexes **1–3** were prepared by following a general procedure. The details are given below for representative **1**: The starting complex [Cl_3Ru(μ-tppz)$RuCl_3$] (100 mg, 0.12 mmol), acetylacetone (30 mg, 0.30 mmol) and NEt_3 (0.2 cm^3, 1.5 mmol) were taken in 20 cm^3 of ethanol, and the mixture was heated to reflux for 16 h under dinitrogen atmosphere. The initial greenish solution gradually changed to deep green. The solvent was then removed under reduced pressure. The dried crude product was purified by using a silica gel (mesh 60–120) column. The green dinuclear complex **1** was eluted by a solvent mixture of CH_3CN–MeOH (6 : 1). Evaporation of solvent under reduced pressure yielded the pure complex **1**.

For **2** and **3** the refluxing time and solvent mixture used for chromatography were 12 h, 24 h and CH_3CN–MeOH (10 : 1), respectively.

1. Yield: 65 mg (60%). $C_{34}H_{30}Cl_2N_6O_4Ru_2$ Anal. Calcd: C, 47.44; H, 3.52; N, 9.77. Found: C, 47.21; H, 3.37; N, 9.52. ESI-MS(+) in CH_3CN, *m*/*z* Calcd for [**1**]$^+$: 859.98; Found: 859.80. ^{1}H NMR [$CDCl_3$, *δ*/ppm (*J*/Hz)]: 8.91 (d, 5.7, 4H), 8.69 (t, 6.9/7.2, 4H), 7.75 (t, 7.2/8.4, 4H), 7.55 (d, 8.2, 4H), 5.42 (s, 2H), 2.61 (s, 6H), 1.44 (s, 6H).

2. Yield: 63 mg (55%). $C_{38}H_{38}Cl_2N_6O_4Ru_2$ Anal. Calcd: C, 49.78; H, 4.18; N, 9.17. Found: C, 49.46; H, 4.15; N, 8.95. ESI-MS(+) in CH_3CN, *m*/*z* Calcd for [**2**]$^+$: 916.04; Found: 915.99. ^{1}H NMR [$(CD_3)_2SO$, *δ*/ppm (*J*/Hz)]: 8.79 (d, 5.1, 4H), 8.74 (d, 8.1, 4H), 8.01 (t, 7.2/9.0, 4H), 7.83 (t, 6.0/6.0, 4H), 5.46 (s, 2H), 2.79 (m, 4H), 1.53 (m, 10H), 0.35 (m, 6H).

3. Yield: 64 mg (50%). $C_{46}H_{54}Cl_2N_6O_4Ru_2$ Anal. Calcd: C, 53.69; H, 5.29; N, 8.17. Found: C, 53.92; H, 5.48; N, 8.38. ESI-MS(+) in CH_3CN, *m*/*z* Calcd for [**3**]$^+$: 1028.17; Found: 1028.44. ^{1}H NMR [$(CD_3)_2SO$, *δ*/ppm (*J*/Hz)]: 8.74 (d, 5.4, 4H), 8.66 (d, 8.4, 4H), 7.99 (t, 6.9/7.8, 4H), 7.81 (t, 5.7/6.3, 4H), 5.55 (s, 2H), 1.55 (s, 18H), 0.28 (s, 18H).

Synthesis of 4 and 5. The starting complex [Cl_3Ru(μ-tppz)-$RuCl_3$] (100 mg, 0.12 mmol), 3-methyl-2,4-pentanedione (35 mg, 0.30 mmol) and KOH (34 mg, 0.62 mmol) were taken in 20 cm^3 of ethanol and the mixture was heated to reflux for 20 h under dinitrogen atmosphere. The initial greenish solution gradually changed to deep green. The solvent was then removed under reduced pressure. The dried crude product was purified by using a silica gel (mesh 60–120) column. The green dinuclear complex **4** was eluted by a solvent mixture of CH_3CN–MeOH (30 : 1). Evaporation of solvent under reduced pressure yielded pure complex **4**.

For the synthesis of **5** the reaction mixture was heated to reflux for 12 h following the same route as for **4**. The solvent mixture CH_3CN–MeOH (6 : 1) was used to elute the pure complex **5** from the silica gel column.

4. Yield: 45 mg (40%). $C_{36}H_{34}Cl_2N_6O_4Ru_2$ Anal. Calcd: C, 48.65; H, 3.86; N, 9.46. Found: C, 48.12; H, 3.33; N, 9.02. ESI-MS(+) in CH_3CN, *m*/*z* Calcd for [**4**]$^+$: 888.01; Found: 888.14. ^{1}H NMR [$(CD_3)_2SO$, *δ*/ppm (*J*/Hz)]: 8.76 (m, 8H), 8.00 (t, 7.6/7.8, 4H), 7.79 (t, 5.9/6.7, 4H), 2.66 (s, 3H), 2.07 (s, 12H), 1.39 (s, 3H).

5. Yield: 51 mg (45%). $C_{38}H_{38}Cl_2N_6O_4Ru_2$ Anal. Calcd: C, 49.78; H, 4.18; N, 9.17. Found: C, 49.54; H, 4.02; N, 8.92. ESI-MS(+) in CH_3CN, *m*/*z* Calcd for [**5**]$^+$: 916.04; Found: 916.12. ^{1}H NMR [$(CD_3)_2SO$, *δ*/ppm (*J*/Hz)]: 8.81 (d, 5.4, 4H), 8.76 (d, 8.4, 4H), 8.00 (t, 7.5/8.4, 4H), 7.80 (t, 5.7/6.9, 4H), 2.70 (s, 6H), 2.33 (m, 4H), 1.41 (s, 6H), 1.04 (t, 6.6/5.4, 6H).

Crystallography

Single crystals were grown by slow evaporation of acetonitrile solution of **1** or **4**, of a 3 : 1 CH_3CN–CH_2Cl_2 solution mixture of **2**, of a CD_3CN solution of **3**, and by slow diffusion of acetonitrile into dichloromethane solution of **5** followed by slow evaporation of the solvent mixture. X-ray diffraction data were collected on OXFORD XCALIBUR-S CCD and BRUKER APEX-II CCD single crystal X-ray diffractometers for **1**, **2**, **3**, **5** and **4′**, respectively. The structures were solved and refined by full-matrix least-squares techniques on F^2 using the SHELX-97 program.[18] The absorption correction was done by the multi-scan technique. All data were corrected for Lorentz and polarization effects, and the non-hydrogen atoms were refined anisotropically. Hydrogen atoms were included in the refinement process as per the riding model. The molecules **1**, **2** and **4′** lie about an inversion centre. One ^{t}Bu group in **3** is disordered. Crystallisation of **4** from moist CH_3CN gave single crystals identified as [$(CH_3CN)_{0.8}(Cl)_{0.2}(L)Ru^{II}$(μ-tppz)$Ru^{II}(L)(CH_3CN)_{0.8}(Cl)_{0.2}$]-$(Cl)_2$·$4H_2O$, **4′** (Fig. S3 and Tables S2 and S3†). The complex molecule **4′** crystallises with two water molecules in the asymmetric unit, of which one is disordered. H-atoms were not fixed

for them, but their contributions have been included in the molecular composition (Table S2†). Compound **5** crystallises with disordered CH_2Cl_2 and C_2H_5OH molecules along with two H_2O molecules, of which one water molecule is disordered. Restraints such as SIMU, DELU, DANG and DFIX were applied to disordered model so that ethanol and dichloromethane (DCM) molecules exhibit appropriate geometry. The disordered CH_2Cl_2 and C_2H_5OH molecules were refined isotropically. The hydrogen atoms of OH groups of ethanol and water molecules could not be located by difference Fourier, but their contributions have been included in the molecular composition (Table 1). The atom C35 in **5** has positional disorder.

Computational details

Full geometry optimisations were carried out using the density functional theory method at the (R)B3LYP level for **1**/**3**, $\mathbf{1}^{2+}/\mathbf{3}^{2+}$ and (U)B3LYP for $\mathbf{1}^{2+}/\mathbf{3}^{2+}$, $\mathbf{1}^{+}/\mathbf{3}^{+}$, $\mathbf{1}^{-}/\mathbf{3}^{-}$.[19] All elements except ruthenium were assigned the 6-31G(d) basis set. The SDD basis set with effective core potential was employed for the ruthenium atom.[20] The vibrational frequency calculations were performed to ensure that the optimised geometries represent the local minima and there are only positive eigen values. All calculations were performed with the Gaussian03 program package.[21] Vertical electronic excitations based on B3LYP optimised geometries were computed for **1**/**3**, $\mathbf{1}^{+}/\mathbf{3}^{+}$, $\mathbf{1}^{2+}/\mathbf{3}^{2+}$ and $\mathbf{1}^{-}/\mathbf{3}^{-}$ using the TD-DFT formalism[22] in acetonitrile using conductor-like polarizable continuum model (CPCM).[23] GaussSum[24] was used to calculate the fractional contributions of various groups to each molecular orbital.

Acknowledgements

Financial support received from the Department of Science and Technology (DST, New Delhi, India), the DAAD, FCI and DFG (Germany), GAASCR (Czech grant IAA400400802) are gratefully acknowledged. X-ray structural studies were carried out at the National Single Crystal X-ray Diffraction Facility, Indian Institute Technology Bombay. Special acknowledgment is made to the Sophisticated Analytical Instrument Facility (SAIF), Indian Institute of Technology, Bombay, for providing the NMR facility. We are grateful to the crystallographic referee for extending the valuable suggestions.

References

1 (*a*) C. Creutz and H. Taube, *J. Am. Chem. Soc.*, 1969, **91**, 3988; (*b*) C. Creutz and H. Taube, *J. Am. Chem. Soc.*, 1973, **95**, 1086.

2 (*a*) W. Kaim and G. K. Lahiri, *Angew. Chem., Int. Ed.*, 2007, **46**, 1778; (*b*) T. Scheiring, W. Kaim, J. A. Olabe, A. R. Parise and J. Fiedler, *Inorg. Chim. Acta*, 2000, **125**, 300; (*c*) D. P. Rillema and K. B. Mack, *Inorg. Chem.*, 1982, **21**, 3849; (*d*) C. H. Braunstein, A. D. Baker, T. C. Strekas and H. D. Gafney, *Inorg. Chem.*, 1984, **23**, 857; (*e*) R. R. Ruminski, T. Cockroft and M. Shoup, *Inorg. Chem.*, 1988, **27**, 4026; (*f*) V. Balzani, A. Juris, M. Venturi, S. Campagna and S. Serroni, *Chem. Rev.*, 1996, **96**, 759; (*g*) A. Gourdon and J.-P. Launay, *Inorg. Chem.*, 1998, **37**, 5336; (*h*) P. Bonhote, A. Lecas and E. Amouyal, *Chem. Commun.*, 1998, 885; (*i*) G. Denti, S. Campagna, L. Sabatino, S. Serroni, M. Ciano and V. Balzani, *Inorg. Chem.*, 1990, **29**, 4750; (*j*) A.-M. Stadler, F. Puntoriero, S. Campagna, N. Kyritsakas, R. Welter and J.-M. Lehn, *Chem.–Eur. J.*, 2005, **11**, 3997; (*k*) W. R. Browne, N. M. O'Boyle, W. Henry, A. L. Guckian, S. Horn, T. Fett, C. M. O'Connor, M. Duati, L. D. Cola, C. G. Coates, K. L. Ronayne, J. J. McGarvey and J. G. Vos, *J. Am. Chem. Soc.*, 2005, **127**, 1229; (*l*) S. Maji, B. Sarkar, S. M. Mobin, J. Fiedler, W. Kaim and G. K. Lahiri, *Dalton Trans.*, 2007, 2411; (*m*) F. Loiseau, F. Nastasi, A.-M. Stadler, S. Campagna and J.-M. Lehn, *Angew. Chem., Int. Ed.*, 2007, **46**, 6144; (*n*) S. Stagni, E. Orselli, A. Palazzi, L. D. Cola, S. Zacchini, C. Femoni, M. Marcaccio, F. Paolucci and S. Zanarini, *Inorg. Chem.*, 2007, **46**, 9126; (*o*) P. Govindaswamy, B. Therrien, G. Süss-Fink, P. Štěpnička and J. Ludvík, *J. Organomet. Chem.*, 2007, **692**, 1661; (*p*) S. Ghumaan, B. Sarkar, M. P. Patil, J. Fiedler, R. B. Sunoj, W. Kaim and G. K. Lahiri, *Polyhedron*, 2007, **26**, 3409; (*q*) B. Therrien, G. Süss-Fink, P. Govindaswamy and C. Saïd-Mohamed, *Polyhedron*, 2007, **26**, 4065; (*r*) J.-M. Herrera, S. J. A. Pope, A. J. H. M. Meijer, T. L. Easun, H. Adams, W. Z. Alsindi, X.-Z. Sun, M. W. George, S. Faulkner and M. D. Ward, *J. Am. Chem. Soc.*, 2007, **129**, 11491; (*s*) S. Xun, J. Zhang, X. Li, D. Ma and Z. Y. Wang, *Synth. Met.*, 2008, **158**, 484; (*t*) J. C. Salsman, C. P. Kubiak and T. Ito, *J. Am. Chem. Soc.*, 2005, **127**, 2382; (*u*) C. H. Londergan, J. C. Salsman, B. J. Lear and C. P. Kubiak, *Chem. Phys.*, 2006, **324**, 57; (*v*) A. Das, T. Scherer, S. Maji, T. K. Mondal, S. M. Mobin, F. A. Urbanos, R. Jiménez-Aparicio, W. Kaim and G. K. Lahiri, *Inorg. Chem.*, 2011, **50**, 7040; (*w*) C.-J. Yao, Y.-W. Zhong, H.-J. Nie, H. D. Abruña and J. Yao, *J. Am. Chem. Soc.*, 2011, **133**, 20720.

3 (*a*) N. S. Hush, *Prog. Inorg. Chem.*, 1967, **8**, 391; (*b*) N. S. Hush, *Coord. Chem. Rev.*, 1985, **64**, 135; (*c*) C. Creutz, M. D. Newton and N. Sutin, *J. Photochem. Photobiol., A*, 1994, **82**, 47.

4 (*a*) *Mixed Valency Systems – Applications in Chemistry, Physics and Biology*, ed. K. Prassides, Kluwer Academic Publishers, Dordrecht, 1991; (*b*) M. Fabre and J. Bonvoisin, *J. Am. Chem. Soc.*, 2007, **129**, 1434; (*c*) D. E. Richardson and H. Taube, *Coord. Chem. Rev.*, 1984, **60**, 107; (*d*) R. J. Crutchley, *Adv. Inorg. Chem.*, 1994, **41**, 273; (*e*) W. Kaim and B. Sarkar, *Coord. Chem. Rev.*, 2007, **251**, 584.

5 (*a*) S. B. Braun-Sand and O. Wiest, *J. Phys. Chem. B*, 2003, **107**, 9624; (*b*) S. B. Braun-Sand and O. Wiest, *J. Phys. Chem. A*, 2003, **107**, 285; (*c*) Y. Wang and M. Lieberman, *IEEE Trans. Nanotechnol.*, 2004, **3**, 368; (*d*) P. Zhao, D. Woolard, J. M. Seminario and R. Trew, *Int. J. High Speed Electron. Syst.*, 2006, **16**, 705; (*e*) C. S. Lent, B. Isaksen and M. Lieberman, *J. Am. Chem. Soc.*, 2003, **125**, 1056.

6 (*a*) J. A. Baumann and T. J. Meyer, *Inorg. Chem.*, 1980, **19**, 345; (*b*) A. F. Heyduk and D. G. Nocera, *Science*, 2001, **293**, 1639; (*c*) G. LeClair and Z. Y. Wang, *J. Solid State Electrochem.*, 2009, **13**, 365.

7 (*a*) R. Ruminski, J. Kiplinger, T. Cockroft and C. Chase, *Inorg. Chem.*, 1989, **28**, 370; (*b*) C. R. Arana and H. D. Abruña, *Inorg. Chem.*, 1993, **32**, 194; (*c*) D. M. Dattelbaum, C. M. Hartshorn and T. J. Meyer, *J. Am. Chem. Soc.*, 2002, **124**, 4938; (*d*) C. M. Hartshorn, N. Daire, V. Tondreau, B. Loeb, T. J. Meyer and P. S. White, *Inorg. Chem.*, 1999, **38**, 3200; (*e*) K. D. Demadis, C. M. Hartshorn and T. J. Meyer, *Chem. Rev.*, 2001, **101**, 2655; (*f*) N. Chanda, R. H. Laye, S. Chakraborty, R. L. Paul, J. C. Jeffery, M. D. Ward and G. K. Lahiri, *J. Chem. Soc., Dalton Trans.*, 2002, 3496; (*g*) N. Chanda, B. Sarkar, J. Fiedler, W. Kaim and G. K. Lahiri, *Dalton Trans.*, 2003, 3550; (*h*) N. Chanda, B. Sarkar, S. Kar, J. Fiedler, W. Kaim and G. K. Lahiri, *Inorg. Chem.*, 2004, **43**, 5128; (*i*) S. Ghumaan, B. Sarkar, N. Chanda, M. Sieger, J. Fiedler, W. Kaim and G. K. Lahiri, *Inorg. Chem.*, 2006, **45**, 7955; (*j*) M. Koley, B. Sarkar, S. Ghumaan, E. Bulak, J. Fiedler, W. Kaim and G. K. Lahiri, *Inorg. Chem.*, 2007, **46**, 3736; (*k*) S. H. Wadman, R. W. A. Havenith, F. Hartl, M. Lutz, A. L. Spek, G. P. M. van Klink and G. van Koten, *Inorg. Chem.*, 2009, **48**, 5685; (*l*) T. Kundu, B. Sarkar, T. K. Mondal, J. Fiedler, S. M. Mobin, W. Kaim and G. K. Lahiri, *Inorg. Chem.*, 2010, **49**, 6565; (*m*) T. Kundu, B. Sarkar, T. K. Mondal, S. M. Mobin, F. A. Urbanos, R. Jiménez-Aparicio, J. Fiedler, W. Kaim and G. K. Lahiri, *Inorg. Chem.*, 2011, **50**, 4753; (*n*) R. C. Rocha, F. N. Rein, H. Jude, A. P. Shreve, J. J. Concepcion and T. J. Meyer, *Angew. Chem., Int. Ed.*, 2008, **47**, 503; (*o*) A. K. Das, B. Sarkar, J. Fiedler, S. Záliš, I. Hartenbach, S. Strobel, G. K. Lahiri and W. Kaim, *J. Am. Chem. Soc.*, 2009, **131**, 8895; (*p*) S. Bernhard, K. Takada, D. J. Díaz, H. Abruña and H. Mürne, *J. Am. Chem. Soc.*, 2001, **123**, 10265; (*q*) S. Fantacci, F. D. Angelis, J. Wang, S. Bernhard and A. Selloni, *J. Am. Chem. Soc.*, 2004, **126**, 9715; (*r*) L. M. Vogler and K. J. Brewer, *Inorg. Chem.*, 1996, **35**, 818; (*s*) S. W. Jones, L. M. Vrana and K. J. Brewer, *J. Organomet. Chem.*, 1998, **554**, 29; (*t*) W. Chen, F. N. Rein, B. L. Scott and R. C. Rocha, *Chem.–Eur. J.*, 2011, **17**, 5595.

8 M. B. Robin and P. Day, *Adv. Inorg. Chem.*, 1967, **10**, 247.

9 (*a*) F. A. Cotton, G. Wilkinson, C. A. Murillo and M. Bochmann, *Advanced Inorganic Chemistry*, John Wiley & Sons, INC., 6th edn, 1999, pp. 479–483; (*b*) D. A. Thornton, *Coord. Chem. Rev.*, 1990, **104**, 173; (*c*) R. C. Mehrotra, R. Bohra and D. P. Gaur, *Metal β-Diketonates and Allied Derivatives*, Academic Press, 1978.

10 S. Kar, N. Chanda, S. M. Mobin, F. A. Urbanos, M. Niemeyer, V. G. Puranik, R. Jiménez-Aparicio and G. K. Lahiri, *Inorg. Chem.*, 2005, **44**, 1571.

11 (*a*) S. Patra, B. Sarkar, S. M. Mobin, W. Kaim and G. K. Lahiri, *Inorg. Chem.*, 2003, **42**, 6469; (*b*) C.-J. Yao, Y.-W. Zhong and J. Yao, *J. Am. Chem. Soc.*, 2011, **133**, 15697.

12 A. Stebler, J. H. Ammeter, U. Fürholz and A. Ludi, *Inorg. Chem.*, 1984, **23**, 2764.

13 (*a*) S. Kar, B. Sarkar, S. Ghumaan, D. Roy, F. A. Urbanos, J. Fiedler, R. B. Sunoj, R. Jiménez-Aparicio, W. Kaim and G. K. Lahiri, *Inorg. Chem.*, 2005, **44**, 8715; (*b*) S. Kar, N. Chanda, S. M. Mobin, A. Datta, F. A. Urbanos, V. G. Puranik, R. Jiménez-Aparicio and G. K. Lahiri, *Inorg. Chem.*, 2004, **43**, 4911; (*c*) D. Kumbhakar, B. Sarkar, S. Maji, S. M. Mobin, J. Fiedler, F. A. Urbanos, R. Jiménez-Aparicio, W. Kaim and G. K. Lahiri, *J. Am. Chem. Soc.*, 2008, **130**, 17575; (*d*) S. Patra, B. Sarkar, S. Maji, J. Fiedler, F. A. Urbanos, R. Jimenez-Aparicio, W. Kaim and G. K. Lahiri, *Chem.–Eur. J.*, 2006, **12**, 489; (*e*) S. Kar, B. Sarkar, S. Ghumaan, D. Janardanan, J. van Slageren, J. Fiedler, V. G. Puranik, R. B. Sunoj, W. Kaim and G. K. Lahiri, *Chem.–Eur. J.*, 2005, **11**, 4901.

14 S. Patra, T. A. Miller, B. Sarkar, M. Niemeyer, M. D. Ward and G. K. Lahiri, *Inorg. Chem.*, 2003, **42**, 4707.

15 W. Kaim, *Coord. Chem. Rev.*, 2011, **255**, 2503.

16 M. Krejcik, M. Danek and F. Hartl, *J. Electroanal. Chem.*, 1991, **317**, 179.

17 W. Kaim, S. Ernst and V. Kasack, *J. Am. Chem. Soc.*, 1990, **112**, 173.

18 G. M. Sheldrick, *SHELX-97, Program for Crystal Structure Solution and Refinement*, University of Göttingen, Germany, 1997.

19 C. Lee, W. Yang and R. G. Parr, *Phys. Rev. B*, 1988, **37**, 785.

20 (*a*) D. Andrae, U. Haeussermann, M. Dolg, H. Stoll and H. Preuss, *Theor. Chim. Acta*, 1990, **77**, 123; (*b*) P. Fuentealba, H. Preuss, H. Stoll and L. V. Szentpaly, *Chem. Phys. Lett.*, 1989, **89**, 418.

21 M. J. Frisch, G. W. Trucks, H. B. Schlegel, G. E. Scuseria, M. A. Robb, J. R. Cheeseman, J. A. Montgomery, Jr., T. Vreven, K. N. Kudin, J. C. Burant, J. M. Millam, S. S. Iyengar, J. Tomasi, V. Barone, B. Mennucci, M. Cossi, G. Scalmani, N. Rega, G. A. Petersson, H. Nakatsuji, M. Hada, M. Ehara, K. Toyota, R. Fukuda, J. Hasegawa, M. Ishida, T. Nakajima, Y. Honda, O. Kitao, H. Nakai, M. Klene, X. Li, J. E. Knox, H. P. Hratchian, J. B. Cross, C. Adamo, J. Jaramillo, R. Gomperts, R. E. Stratmann, O. Yazyev, A. J. Austin, R. Cammi, C. Pomelli, J. W. Ochterski, P. Y. Ayala, K. Morokuma, G. A. Voth, P. Salvador, J. J. Dannenberg, V. G. Zakrzewski, S. Dapprich, A. D. Daniels, M. C. Strain, O. Farkas, D. K. Malick, A. D. Rabuck, K. Raghavachari, J. B. Foresman, J. V. Ortiz, Q. Cui, A. G. Baboul, S. Clifford, J. Cioslowski, B. B. Stefanov, G. Liu, A. Liashenko, P. Piskorz, I. Komaromi, R. L. Martin, D. J. Fox, T. Keith, M. A. Al-Laham, C. Y. Peng, A. Nanayakkara, M. Challacombe, P. M. W. Gill, B. Johnson, W. Chen, M. W. Wong, C. Gonzalez and J. A. Pople, *Gaussian 03(Revision D.01)*, Gaussian Inc, Wallingford, CT, 2004.

22 (*a*) R. Bauernschmitt and R. Ahlrichs, *Chem. Phys. Lett.*, 1996, **256**, 454; (*b*) R. E. Stratmann, G. E. Scuseria and M. J. Frisch, *J. Chem. Phys.*, 1998, **109**, 8218; (*c*) M. E. Casida, C. Jamorski, K. C. Casida and D. R. Salahub, *J. Chem. Phys.*, 1998, **108**, 4439.

23 (*a*) V. Barone and M. Cossi, *J. Phys. Chem. A*, 1998, **102**, 1995; (*b*) M. Cossi and V. Barone, *J. Chem. Phys.*, 2001, **115**, 4708; (*c*) M. Cossi, N. Rega, G. Scalmani and V. Barone, *J. Comput. Chem.*, 2003, **24**, 669.

24 N. M. O'Boyle, A. L. Tenderholt and K. M. Langner, *J. Comput. Chem.*, 2008, **29**, 839.

